Energetic Particles Related with Coronal and Interplanetary Shocks

N. Gopalswamy

NASA Goddard Space Flight Center, Greenbelt, MD 20771, USA
gopals@ssedmail.gsfc.nasa.gov

Abstract. Acceleration of electrons and ions at the Sun is discussed in the framework of CME-driven shocks. Based on the properties of coronal mass ejections associated with type II bursts at various wavelengths, the possibility of a unified approach to the type II phenomena is suggested. Two aspects of primary importance to shock accelerations are: (1) Energy of the driving CME and (2) the conditions in the medium that supports shock propagation. The high degree of overlap between CMEs associated with large solar energetic particle events and type II bursts occurring at all wavelengths underscores the importance of CME energy in driving shocks far into the interplanetary medium. Presence of preceding CMEs can alter the conditions in the ambient medium, which is shown to influence the intensity of large solar energetic particle events. Both statistical evidence and case studies are presented that underscore the importance of the ambient medium.

1 Introduction

The Sun contributes enormously to the energetic particle population in the heliosphere through various processes: Flares, coronal mass ejections (CMEs), and corotating interaction regions. Electrons are accelerated up to hundreds of MeV; ions are accelerated up to many GeV (see, e.g., [41]). Electrons with energies exceeding 100s of keV produce gyrosynchrotron emission in the microwave to millimeter wavelength range, while the MeV electrons produce gamma-ray continuum. Energetic ions produce very little electromagnetic signatures, except for enhanced nuclear gamma-ray line emissions resulting from the bombardment of the solar surface by accelerated ions. Hard X-ray emission is a common flare signature produced by tens of keV electrons precipitating into the chromosphere from the acceleration site in the corona. Hard X-ray emission is also produced in the corona if the coronal density is high enough to cause thin target bremsstrahlung. Both electrons and ions leaving the Sun are also detected by spacecraft in the solar wind. Very high energy protons occasionally reach Earth's atmosphere, whose effects are detected at the ground level by neutron monitors [36, 43].

N. Gopalswamy: *Energetic Particles Related with Coronal and Interplanetary Shocks*, Lect. Notes Phys. **725**, 139–160 (2007)
DOI 10.1007/978-3-540-71570-2_7

All the nonthermal radio emissions from the Sun are due to accelerated electrons (from a few to 100s of keV energy). Microwave emission during eruptions typically comes from closed loops trapping high energy (100s of keV) electrons. Radio emissions at decimetric and longer wavelengths typically correspond to energetic electrons flowing away from the Sun either from the flare site or from the front of a fast mode MHD shock. Electrons accelerated at shock fronts result in type II radio bursts. Type III radio bursts result from beams of energetic electrons via the beam-plasma instability. Type III bursts occurring without an associated type II are likely to be accelerated at the flare site, but when they occur in association with a type II, the situation is not clear: the electrons may originate in the flare site or at the front of a CME-driven shock (see [3, 54] and references therein). Another related issue is the source of near-relativistic beam-like electrons detected in situ: from the observed time delay of these high-energy electrons with respect to the onset time of the complex type III bursts [27] and the height of the CME at the estimated electron release time, it was concluded that the CME-driven shock is the source of electrons [56].

Ions propagating away from the Sun produce little electromagnetic signatures, so they have to be detected only when they arrive at the observer. Observing the interplanetary type II bursts in association with ions provides information on the shocks that might accelerate the ions. This article focuses on the energetic electrons (that produce type II radio bursts) and ions associated with shocks and CMEs, with a tacit assumption that CME-driven shocks accelerate both electrons and ions. The generation of shocks by CMEs and their propagation through the interplanetary medium are the two primary aspects discussed in this article because they seem to decide the particle output from the shock. The ions discussed in this paper constitute the so-called large solar energetic particle (SEP) events, clearly associated with fast and wide CMEs (see [35, 52] for recent reviews). The large SEP events are also known as gradual SEP events, as opposed to impulsive SEP events, which are of much lower intensity and short-lived. The large SEPs are thought to be accelerated by CME-driven shocks by a shock-drift or diffusive shock acceleration mechanism depending on the geometry of the shock front with respect to the upstream magnetic field. The impulsive particles (see [52]), on the other hand, are thought to be accelerated in the flare reconnection region (see, e.g., [9]). Flares always accompany fast and wide CMEs, so the SEPs may be accelerated in these flares also. How these two processes contribute to the observed interplanetary population of SEPs is not clear. The flare component may be unimportant compared to the shock component [53]. In fact, the largest impulsive event of cycle 23 (April 14, 2001) had an intensity <2 pfu (particle flux unit, 1 pfu = 1 particle per (cm^2 s sr)), five times smaller than the weakest of the gradual SEP events (10 pfu) [21]. The flare component may also be reaccelerated by the associated CME shock to produce charge state and composition different from pure CME events [60].

2 Type II Radio Bursts and Shocks

Type II radio bursts appear as slowly drifting features in the frequency-time plane, a classic representation of radio observations known as the dynamic spectrum. The slow-drift nature was first recognized by Payne-Scott and coworkers [50] at frequencies below 150 MHz and later classified as type II bursts [63]. Extensive literature is available on metric type II bursts that were observed at frequencies above the ionospheric cutoff (∼20 MHz) [48]. Type II bursts in the interplanetary (IP) medium were first detected using spaceborne radio instruments in the early 1970s [44]. The radio emission occurs at the local plasma frequency and its harmonic. Since the local plasma frequency is proportional to the square root of the density, observing type II bursts at various frequencies provides a means of probing various layers of the inner heliosphere. The IP type II bursts also present a strong evidence for particle acceleration far away from the Sun.

The shocks are very strong near the Sun and weaken as they propagate into the heliosphere (see, e.g., [64]), many of them continuing to accelerate particles at 1 AU and beyond. The continued acceleration is inferred from energetic storm particle (ESP) events [51] observed as an enhancement of the particle intensity as the IP shock moves past an observing spacecraft. The shock arrival is also detected as the sudden increase in the frequency of the local plasma line (the low-frequency radio continuum noise) due to the density jump in the shock [28]. Type II bursts observed at frequencies close to the plasma frequency in the vicinity of the spacecraft [1, 38] is another strong evidence for electron acceleration at the location of the observing spacecraft. Whenever the shock is strong enough to accelerate electrons, it can produce a type II burst, irrespective of the distance from the Sun. Figure 1 shows a type II burst observed by the Unified Radio and Plasma Wave (URAP) experiment on board the Ulysses spacecraft. The burst originated from a solar eruption on 2001 May 07 and lasted for three days until the shock arrived (identified as the jump in the local plasma frequency) at the spacecraft on 2001 May 10 (see [57] for details).

The starting frequency of type II bursts is typically below 150 MHz, although higher frequency type II bursts are occasionally observed [61]. The starting frequency is indicative of the distance from the eruption site at which the shock forms. The starting frequency of 150 MHz corresponds to a heliocentric distance of ∼1.1 $R_\odot$. Type II bursts observed just above the ionospheric cut-off (15–20 MHz) depart from a distance of ∼2.4 $R_\odot$ from the Sun. These distances are based on the Newkirk density model [49] and hence should be considered representative. Thus ground based instruments can observe only the earliest phase of the shocks (propagating over only a small distance of ∼1$R_\odot$). Early IP observations were made at frequencies ≤2 MHz, so the IP type II bursts were referred to as kilometric (km) because most of the frequency band corresponded to wavelengths in this range. The nominal heliocentric distance of the 2 MHz plasma level is ∼20$R_\odot$. The frequency gap

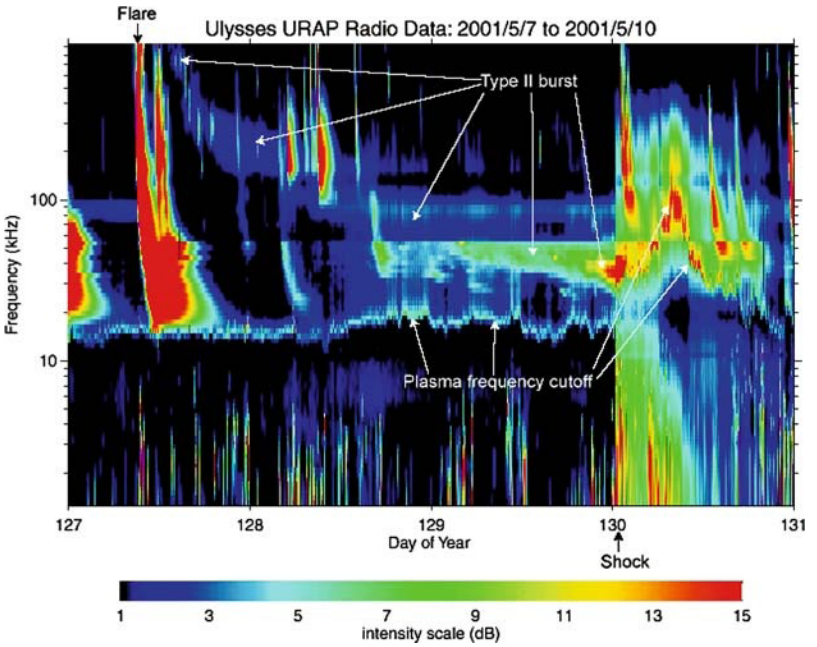

Fig. 1. Dynamic spectrum showing a strong type II burst observed by Ulysses URAP instrument. The start of the solar eruption on 2001 May 07 (DOY 127) and the arrival of the shock on 2001 May 10 (DOY 130) are marked by arrows. Note that the local plasma frequency jumps from ∼12 kHz to >100 kHz at the arrival of the shock, which corresponds to a density jump by a factor of ∼3. See [57] for details. (Courtesy: R. MacDowall)

between 2 and 20 MHz between the IP and metric type II bursts was a source of confusion on the relation between type II bursts in the two domains. The Radio and Plasma Wave (WAVES) experiment on Wind spacecraft [2], essentially filled this gap leading to a significant progress made in understanding the type II bursts.

Information on type II bursts available in various wavelength domains can be combined to produce the schematic in Fig. 2. Each slanted line represents a type II burst: 1) Bursts confined to the metric domain. 2) Bursts starting in the metric domain and ending in the DH domain. 3) Bursts confined to the DH domain. 4) Bursts starting in the DH domain and continuing to the km domain. 5) Bursts starting in the metric domain and having counterparts in all wavelength domains. 6) Bursts found only in the km domain. CMEs associated with the metric type II bursts are of the lowest energy, but are more energetic than the general population of CMEs [40]. On the other hand CMEs associated with DH type II bursts (combining varieties 2, 3, and 4) are more energetic than those associated with the metric type II bursts. The highest energy is possessed by CMEs associated with type II bursts occurring

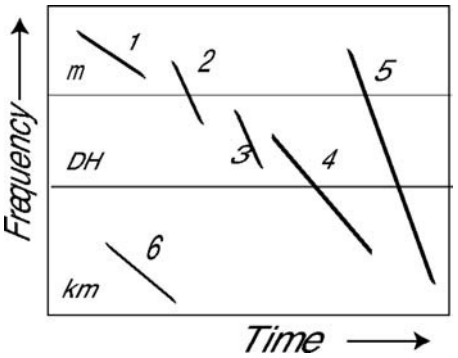

Fig. 2. Schematic dynamic spectra of type II bursts in various wavelength domains (m - metric, DH - decameter-hectometric, km - kilometric). Six varieties of type II bursts can be observationally distinguished on the basis of the wavelength domain in which they occur: 1. confined to the metric domain, 2. starting in the metric domain and ending in the DH domain, 3. confined to the DH domain, 4. starting in the DH domain and ending in the km domain, 5. starting in the metric domain and ending in the km domain, 6. confined to the km domain

at all wavelengths (variety 5). This ordering of CME properties is illustrated in Fig. 3: the speed, width and deceleration of CMEs progressively increase from the general population to those associated with m, DH, and m-to-km type II bursts. This hierarchical relationship between CMEs and type II bursts suggests that the two phenomena are closely related. The purely kilometric type II bursts (variety 6 in Fig. 3) are also associated with CMEs, but they are not as energetic as the all-wavelength type II bursts. Figure 4 shows that the average speed and width of CMEs associated with pure km type II bursts is similar to those of the metric type II CMEs, but the acceleration is positive and much higher (4 m s^{-2}). The positive acceleration implies that the associated CMEs are not super-Alfvenic near the Sun and become super-Alfvenic at large distances from the Sun due to prolonged acceleration. Statistical studies indicate that the slowest CMEs generally show positive acceleration within the LASCO field of view [11, 15]. The propelling force must be acting over large heliocentric distances in these CMEs, which are mostly associated with prominence eruptions. The purely km type II bursts are likely due to shocks that are slightly more energetic than the radio-quiet shocks detected at 1 AU [13, 14]. It must be pointed out that the ISEE 3 type II bursts are likely to be similar to varieties 4 and 5 observed below 2 MHz [4], and not the purely km type II bursts.

Type II bursts is a relatively rare phenomenon [10]: the Solar and Heliospheric Observatory (SOHO) mission's Large Angle and Spectrometric Coronagraph (LASCO) had recorded nearly 7000 CMEs over a period of 7 years (1996–2002), while only 736 metric type II bursts and 350 DH type II bursts were reported over the same period. Thus, not more than ∼10% of

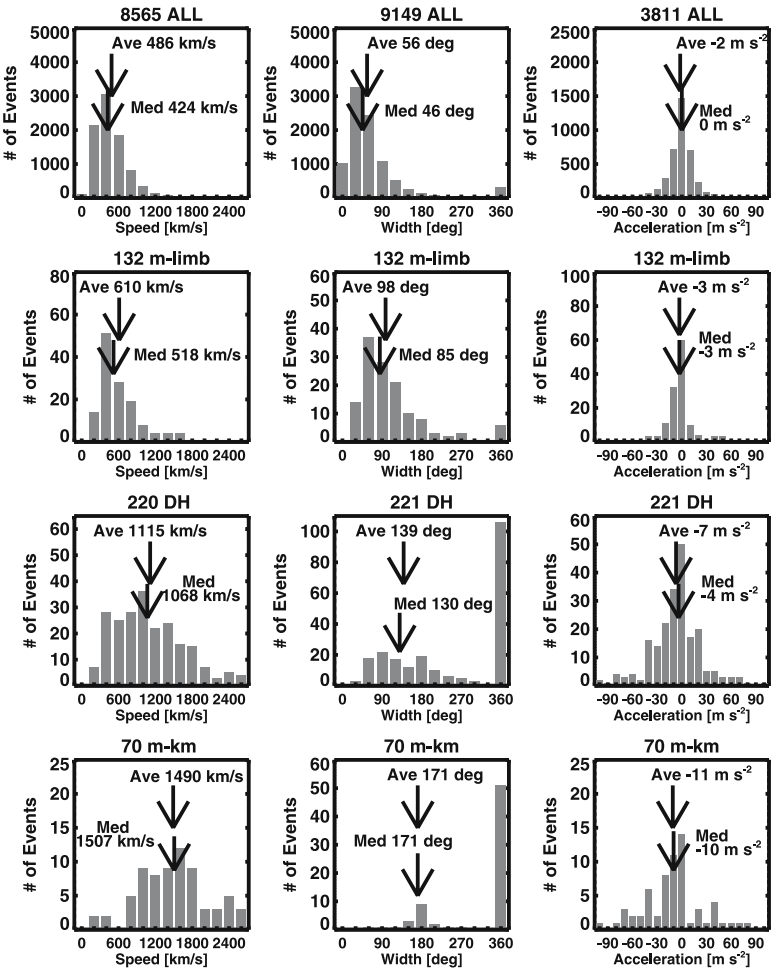

Fig. 3. Speed, width, and acceleration of the four populations of CMEs: the general population (ALL, 1996–2004), the metric type II associated (m-limb), The DH type II associated (DH), and m-to-km type II associated (m-km). The average and median values of the distributions are shown. The average widths were obtained by excluding the full halo CMEs (the last bin in the width histograms). The DH type II bursts represent the combined set, irrespective of the presence of counterparts in other wavelength domains. Type II bursts in the metric domain have their solar sources within 30° from each limb, so that the CME identification is straight forward. Note the progressive shifting of the arrows to the right as one goes from top to bottom rows. In the last column, the arrows shift to the left because the acceleration becomes more negative (deceleration). Note also the increase in the number of full halo CMEs as one goes from the top to bottom in the width column. The average and median widths were computed based on non-halo CMEs

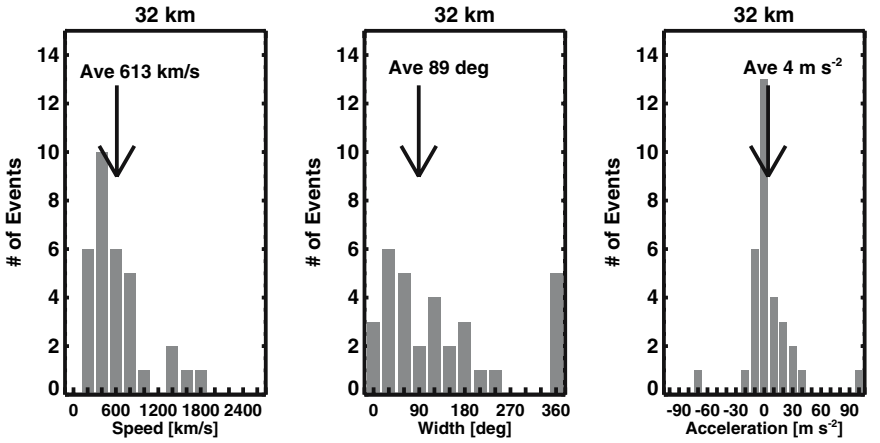

Fig. 4. Speed, width, and acceleration of 32 CMEs associated with purely kilometric type II bursts observed by Wind/WAVES. The average values of the distributions are shown. Note that the acceleration of these CMEs is positive, compared to the other populations shown in Fig. 3

the CMEs are associated with metric type II bursts and not more than ∼5% are associated with IP type II bursts. Interestingly, the number of fast (speed $\geq$ 900 km s^{-1}) CMEs is ∼450, similar to the number of DH type II bursts. The numbers do not match exactly because some fast CMEs are not associated with type II bursts while some slower CMEs are associated with type II bursts. Detailed comparison between the occurrence rates of metric and DH type II bursts averaged over Carrington rotation (CR) periods showed much larger discrepancies [10]. For example, CR 1943 had no DH type II bursts, but had a dozen metric type II bursts. Such differences can be explained in terms of the mean speed of the CMEs.

There is a general agreement that the type II varieties 2–6 in Fig. 3 are due to CME-driven shocks. The purely metric type II bursts (variety 1) have been attributed to flare blast waves and CME-driven shocks. The CME-shock possibility was proposed [58] immediately after the discovery of white-light CMEs, but several difficulties arose with the idea stemming from (i) the type II position with respect to the CME, (ii) the relative speeds and directions of the CME and type II, and (iii) CME association. The severest of these problems is the observation of CMEless metric type II bursts [33, 55]: about one third of the metric type II bursts lacked CMEs. These observations became strong pillars supporting the idea that at least some metric type II bursts are of non-CME origin. Reanalysis of the past data which had identified the CMEless metric type II bursts, led to the conclusion that the CMEless type II bursts predominantly originated from the disk center [6]. It is difficult to detect CMEs from the disk center because of the occulting disk employed in coronagraphs to block the direct sunlight. This was also confirmed for a set of

disk-center metric type II bursts that lacked CMEs, but were associated with EUV eruptive signatures [14]. Thus, the evidence for the existence of CMEless type II bursts has been considerably weakened. Therefore, one can say that the type II bursts, irrespective of the wavelength of occurrence, is essentially a CME-related phenomenon.

3 Type II Bursts and SEP Events

CMEs were found to be a necessary requirement for the production of SEPs, which led to the suggestion that SEPs are accelerated by the shocks ahead of CMEs [32]. Early studies also indicated a good association between type II radio bursts and SEPs [4, 59]. The utility of Type II bursts in studying SEPs hinges on the assumption that both phenomena result from CME-driven shocks. Type II bursts indicate the departure of shocks near the Sun, so their starting time is likely to be the earliest time SEPs are released. The occurrence rate of large SEP events (proton flux in the >10 MeV channel $\geq$10 pfu) is similar to that of the DH type II bursts, when averaged over Carrington rotation period; the rate is also not too different from that of shocks detected in situ [10]. This suggests that the same shock accelerates electrons and protons. Furthermore, all (100%) large SEP events of cycle 23 were found to be associated with DH type II bursts, while only 80% were associated with metric type II bursts [19]. For lower energy SEP events, the association rate was lower for DH type II bursts, while the metric type II association rate remained roughly the same [7]. Purely metric events were found to be associated with only small SEP events. The efficiency of the shocks in accelerating particles is likely to increase with heliocentric distance, reaching a maximum above $\sim 3R_{\odot}$ owing to the shape of the radial profile of the Alfven speed [14]. At these heights, most CMEs would have attained their maximum speeds before decelerating due to coronal drag.

It must be remembered that the occurrence of metric type II bursts is not a sufficient condition for the occurrence of SEP events (see, e.g., [30]). However, when we consider type II bursts occurring at all wavelengths (variety 6 in Fig. 2), the SEP association becomes very high. In fact, the CME properties of m-to-km type II bursts and SEP events are almost identical (compare the last row of Fig. 3 with Fig. 5). The overlap between the two sets of events is $\sim$80% [25]. The lack of 100% overlap can be attributed to the difference in source longitudes: Type II bursts can be observed from CMEs originating from all longitudes (including some slightly behind the limb), while SEPs can be detected only when they have access to the field lines connecting to the observer. The association between type II bursts and SEP events also depends on the efficiency of particle acceleration, which, in turn depends on the CME energy and the properties of the ambient medium.

The strongest observational support to the paradigm that large SEP events are due to CME-driven shocks comes from the correlation between SEP

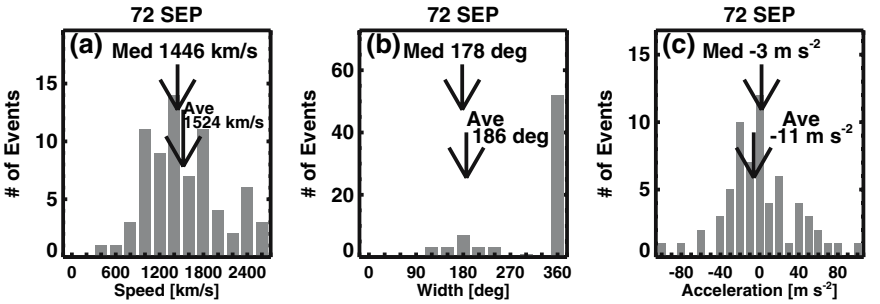

Fig. 5. Speed, width, and acceleration of 72 CMEs associated with large SEP (LSEP) events of cycle 23 (1996–2004). The average and median values of the distributions are shown. Note that the CME properties are nearly identical to those of m-to-km type II bursts (see last row of Fig. 3)

intensity and CME speed [20, 31, 34, 52]. However, the correlation is not perfect, with 3–4 orders of magnitude variation in SEP intensity for a given CME speed. Presence of SEPs in the ambient medium and the spectral variation among SEP events have been proposed as possible factors that could account for one to two orders of magnitude variation in the SEP intensity [31]. Variation in the coronal and IP environment of SEP-producing CMEs may also affect their intensity to a significant extent [20, 23, 24]. SEP intensity may be affected by the presence of turbulence in the vicinity of the shock and in the ambient medium, connectivity of the shock to the observer and the geometry of the shock in the region that is connected to the observer. Most of

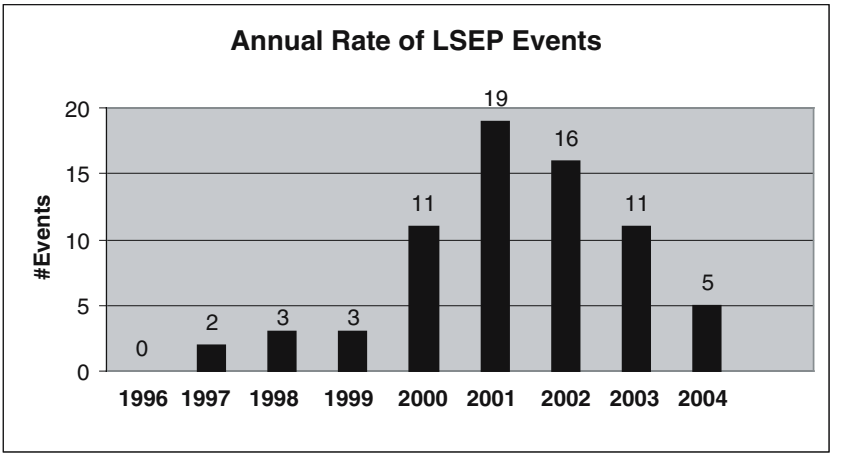

Fig. 6. Annual rate of large SEP (LSEP) events for solar cycle 23 (1996–2004). The actual numbers are indicated at the top of each bin. There was no event in 1996. The largest number (19) was in 2001

these are related to the presence of preceding CMEs in the ambient medium when a powerful shock is launched. The average rate of CMEs near the solar maximum can be as high as 6 per day, so large shocks are likely to encounter preceding CMEs on their path between Sun and Earth. The sharp increase in the number of large SEP (LSEP) events during solar maximum is indicative of such shocks (see Fig. 6). In order to see the effect of preceding CMEs, let us first look at two case studies that illustrate the influence of preceding CMEs on the intensity of large SEP events.

4 CME Interaction

Enhanced radio emission around the time of interaction between two CMEs has been one of the important discoveries of the Wind/WAVES experiment, which was possible due to the simultaneous availability of the radio and white-light observations from SOHO/LASCO [16, 18]. The field of view of SOHO/LASCO (2-32 $R_\odot$) roughly corresponds to the WAVES/RAD2 spectral range (1–14 MHz), which made it easier to visualize the CME interaction at the time of radio enhancement. One of the key results of the interaction studies is that the radio enhancement occurs tens of minutes before the intersection of the leading-edge height-time plots of the two CMEs. This early start is also an indication of the shock ahead of the follower CME penetrating the preceding CME. Most interaction signatures documented so far last for $\leq$ 1h, depending on the size of the preceding CME and the speed of the follower CME. Once the shock traverses the preceding CME, it may merge with the shock of the preceding CME if the latter has one. Beyond that point, the shock propagates through the normal solar wind. Behind the shock is the resultant of the two CMEs, whose final form depends on the relative orientation of the magnetic fields in the two CMEs. The scenario described above can be thought of as an extreme case of shock interaction with inhomogeneities in the ambient medium. Preceding CMEs can be thought of as inhomogeneities in the plasma density (n) and magnetic field (B). Depending on the strength of these inhomogeneities (dB, dn), the effective Alfven speed ahead of the shock can change significantly, thus affecting the strength of the shock. The Alfven speed (V_a) in the medium changes by an amount dV_a according to:

$$\frac{dV_a}{V_a} = \frac{dB}{B} - \frac{1}{2}\frac{dn}{n} \tag{1}$$

This simple expression describes various possibilities that may be useful in understanding the observed type II and SEP phenomena. Coronagraphs are sensitive to the mass in the corona because the underlying mechanism is Thomson scattering by electrons. A preceding CME is a density enhancement ($dn > 0$), so it presents a medium of lower Alfven speed to the follower shock, provided, the magnetic field is not enhanced significantly. This is only an assumption because we do not have direct magnetic field measurements in

the corona or CMEs. If $dn/n > 2dB/B$, then the Alfven speed decreases, making the Alfvenic Mach number of the shock $M_a = V_s/V_a$ increase (V_s is the shock speed). The net effect is a stronger shock for the duration of transit through the preceding CME. The shock may not become stronger if the magnetic field is also enhanced. On the other hand if the shock encounters a depletion region ($dn < 0$) the shock can weaken because the local Alfven speed increases. This latter effect may be one of the reasons for the lack of type II radio burst association for a large number of fast and wide CMEs (see later). During the solar maximum phase, the CME rate could be as high as 6 per day, so one can expect fast shocks passing through CMEs of various sizes.

5 CME Interaction and SEPs: Case Studies

We discuss two SEP events in which the unusual SEP intensity can be attributed to the conditions in the corona and IP medium.

5.1 The 2001 April 14-15 Events

Two successive SEP events associated with fast and wide CMEs on 2001 April 14 and 15 occurred from active region 9415 [21]. The weak SEP event of April 14 (SEP1) was associated with an 830 km s^{-1} CME (CME1) and an M1.0 flare; it was the largest impulsive event of cycle 23. The April 15 event (SEP2) was three orders of magnitude more intense ($\sim$1000 pfu) than the April 14th event (~ 2 pfu) and was associated with a faster CME (CME2, 1200 km s^{-1}) and an X14.4 flare. SEP2 was a large gradual event consistent with the SEP flux (Ip) - soft X-ray flare size (Ix W m^{-2}) relationship [20]:

$$log(Ip) = 4.86 + 0.63log(Ix) \; . \tag{2}$$

According to this relation, the M1.0 flare should result in an Ip of 50 pfu, while the X14.4 flare should be associated with an Ip of 1.2×10^3 pfu. The observed Ip is quite close to the statistical value for the X-flare, but smaller by an order of magnitude for the M flare. On the other hand, the proton intensity and CME speed (V km s^{-1}) are related by [20],

$$log(Ip) = -9.08 + 3.7log(V) \; , \tag{3}$$

which suggests that CME1 and CME2 should have yielded an Ip of 43 and 206 pfu, respectively. Thus, SEP2 had much higher flux than expected from Eq. (3). The eruption configuration itself was quite similar in both CMEs. Both had metric type II bursts, but only the second SEP event had an IP type II burst. The main differences between the two events were: (i) the CME speed (830 vs 1200 km s^{-1}), (ii) connectivity to Earth (W72 vs W84), (iii) associated flare size (M1.0 vs X14.4), (iv) association of IP type II burst (no vs yes) and (iv) the occurrence of preceding CMEs (no vs yes). We suggest that

the occurrence of CME1 and the associated flare might have influenced the resulting intensity of SEP2 by providing seed particles and an environment conducive for efficient shock acceleration.

5.2 The 2002 July 20-23 Events

We compare three large eruptions from AR 0039, two on 2002 July 20 and one on July 23 (see [42] for details on this eruption). The region was ∼10° behind the east limb at the time of the July 20 flares while it was at S13E74 at the time of the July 23 flare. We refer to the corresponding CMEs as CME1, CME2, and CME3. Height-time measurements yielded an average speed of 1357, 2017, and 2180 km s^{-1}, respectively for CME1, CME2, and CME3. CME1 had a width of about 73° and did not show substantial lateral expansion. CME2

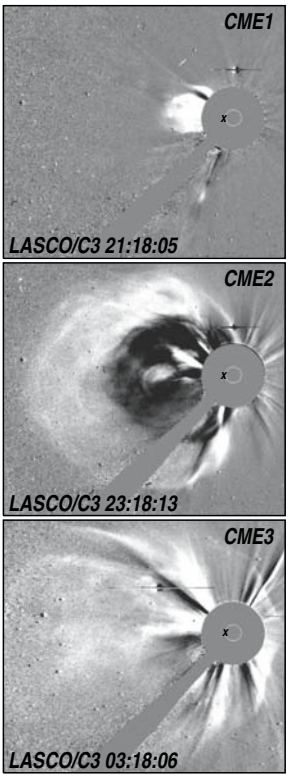

Fig. 7. Difference images of the July 20 and 23 CMEs. **Top**: CME1 (21:18 UT on July 20, 2002), **Middle**: CME2 (23:18 UT on July 20), **Bottom**: CME3 (03:18 UT on July 23, 2002). The C3 occulting disk (*shown as the gray circle in each image*) has a radius of 3.7 $R_\odot$. The northern section of CME2 is bright probably because it has merged with CME1 at this location. The locations of the flares are marked by 'x' close to the east limb in each case

and CME3 expanded considerably and became asymmetric halo events (faint extensions can be seen above the west limb in the middle and bottom images of Fig. 7). CME1 was overtaken by CME2 within the C3 field of view, so we see the merger of CME1 and CME2 in the middle panel of Fig. 7. Note that CME2 and CME3 are very similar in appearance.

Proton intensities as measured in the > 10 and > 30 MeV channels of the ACE/SIS instrument are plotted in Fig. 8. The intensities in both channels were elevated from normal background levels prior to the slow rise following the July 20 CMEs. They both reached a broad peak around 09:00 UT on July 22 and continued at this level past the onset time of the July 23 CME. The rise time was about 37 hours, typical of east limb events. In the higher energy (> 30 MeV) channel, the intensity peaked slightly before that in the > 10 MeV channel and declined monotonically thereafter. On the other hand, the July 23 eruption was not associated with a similar particle increase. There was an impulsive peak on July 24 at 13:00 UT, but it is small and short-lived compared to the main event. There was a small peak around 13:00 UT on July 25, which coincided with an IP shock detected in situ by SOHO, ACE and Wind. This shock is likely to be associated with the July 23 CME. We are confident that the large SEP event was due to CME2 because no other CME of importance occurred during the rising phase of the SEP event. Only two other CMEs were noted between the onset of CME2 and the peak of the SEP event (09:00 UT on July 22): (i) a large blob structure along a streamer in the northeast on July 21 at 02:30 UT, and (ii) a fairly faint loop from the south on July 22 at 09:30 UT. The speeds of these CMEs were not high enough to drive shocks and their locations were not favorable for producing SEP events at the Earth.

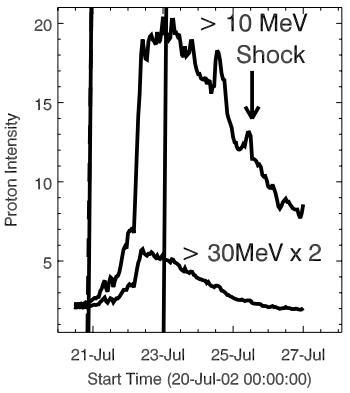

Fig. 8. Intensity of protons in units of $(\text{cm}^2\ \text{s sr MeV})^{-1}$ in the >10 MeV and >30 MeV channels as marked. The >30 MeV intensities have been multiplied by a factor of 2. The height-time plots (*the vertical lines*) of the three CMEs at the Sun are also shown. Note that the first two CMEs are so close in time that the height-time plots cannot be seen distinctly. The vertical arrow points to the arrival time of the IP shock at ACE from the July 23 CME

Was there an SEP event associated with the July 23 CME? All we see is a small blip at ∼12UT on July 24 on the decaying profile of the previous event. By shifting the SEP profile of the July 20 event to the onset time of CME3, one can confirm that this small blip is likely to be the SEP event associated with the July 23 CME. If we subtract the decaying profile of the July 20 SEP event, the intensity level can be inferred to be an order of magnitude smaller. Mars was located directly behind the Sun at the time of the July events (the Earth-Sun-Mars angle was ∼169°). The particle observation at Mars was similar to that at Earth: the July 20 CME was associated with a significant SEP event at Mars, while the July 23 event was not (D. Mitchell 2004, private communications). What factors could have been responsible for the lack of SEPs during the July 23 event? When we looked at the coronal and IP environment of the two events, we found a marked difference: The July 20 CME (CME2) was preceded within an hour by CME1 from the same active region (AR 0039) and the two CMEs seem to have interacted within the coronagraph field of view. Furthermore, the July 20 event was preceded by two other big events on July 19, which might have distorted the field lines overlying AR 0039. Thus the coronal environment of the July 20 CME-driven shock was vastly different from that of the July 23 shock.

6 SEP Intensity Variation: Statistical Study

The two case studies presented above suggest that the coronal and IP environment of fast and wide CMEs may play an important role in determining the intensity of the associated SEP events [18, 20]. What emerges from these studies is that the intensities of SEP events may be ordered by the presence of preceding CMEs in the near Sun IP medium. A recent study [23] identified the primary CME and the solar source region for each of the large SEP events during 1996–2002. Based on the occurrence of preceding CMEs within a day ahead of the primary CMEs, the SEP events were grouped as: (1) those with preceding wide CMEs (P events), (2) those without preceding wide CMEs (NP events), and (3) those, which do not belong to P or NP events either because of a possible preceding CME that was overtaken by the primary CME below the coronagraph occulting disk or the primary CME interacted with a nearby streamer (O events). Only preceding CMEs originating from the same active region as the primary CME were considered. The CME and flare properties of the three groups of events are summarized in Table 1. The median intensity (Ip) of the >10 MeV protons is smallest for the NP events and largest for the P events (column 2 in Table 1). However, most of the CME properties of the P and NP events are similar: The speeds are virtually the same, but the SEP intensities differ by an order of magnitude. The masses are similar and hence the kinetic energies are also similar for the P and NP events. Note also the larger flare size and active region area for the P events, compared to the NP events (see Sect. 7).

Table 1. Properties of Eruptions associated with P, NP, and O events

Group	Ip (pfu)	V (km s^{-1})	M (10^{15} g)	KE (10^{31} erg)	Flare Size	AR Area (msh)
ALL	54	1379	9.0	8.5	M7.1	770
P	210	1300	8.1	7.1	X2.1	880
O	91	1385	11.3	8.5	M2.3	620
NP	29	1379	9.6	10.0	M3.9	500

The scatter plot between CME speed and SEP flux is shown in Fig. 9, with the three populations (P, NP, and O) distinguished. We have plotted 30 P, 14 NP, and 13 O events that had solar sources on the frontside of the Sun. The overall correlation coefficient (r) is 0.57, similar to values obtained by others [20, 31]. The O events had the highest correlation (r = 0.74) followed by P events (r = 0.64) and the NP events (r = 0.36). Note that the NP events occupy the bottom portion of the plot area (very low intensity), while the P and O events had higher intensity (see also Table 1). The combined set of O and P events had a correlation of 0.67, which is better than that of the NP events by 54%. The correlation also improved when backside events were excluded. Combining the P and O events, we see that for the majority of SEP

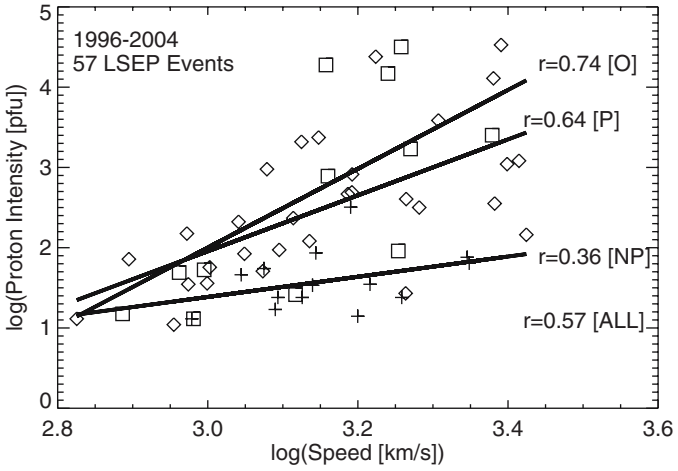

Fig. 9. Scatter plot between SEP intensity (*pfu*) and CME speed (km s^{-1}) in logarithmic units for 57 frontside events (1996–2004). The P (*square*), O (*diamond*) and NP (*triangle*) events are distinguished. Note that most of the NP events had intensity less than 100 pfu, whereas many of the P and O events had intensity exceeding 1000 pfu. The correlation coefficient for all the SEP events is 0.57, while it is higher for the P (r = 0.64) and O (r = 0.74) events. The NP events had the lowest correlation coefficient (r = 0.36). The regression lines for the three groups of events are also shown by the straight lines

events (43/57 or 75%), the primary CMEs propagated through the aftermath of preceding CMEs, and not through the normal solar wind. The scatter is also reduced when the P and NP populations are considered separately, so it can be concluded that the preceding CMEs is a source of scatter in the CME speed – SEP intensity plots (see [31] for other sources of scatter).

7 SEP Intensity and Active Region Area

In Table 1, we saw that the flare size of the P events is higher than that of the NP events. Is it possible that the intensity variation may have something to do with the properties of the source region? One way to look at this is to examine the active region area. Larger active regions can store greater amounts of free energy resulting in larger eruptions. To do this, we selected all the active regions that had at least one large SEP event during disk passage [24]. We obtained the area information (in units of millionths of solar hemisphere – msh) for all the regions from the Solar Geophysical Data. Figure 10(a) shows the distribution of AR areas associated with the SEP events. Most of the regions had areas < 900 msh. The median areas of the P, O, and NP events were not too different (see Table 1).

The X-ray flare size is reasonably correlated with the active region area (correlation coefficient r=0.61, see Fig. 10(b)). There is also a weak correlation between the CME speed and active region area (r = 0.38, see Fig. 10(c)). In other words, the flare size seems to be closely tied to the active region area as compared to the CME speed. The regression line for the flare size (Ix W m^{-2}) – active region area (A msh) scatter plot in Fig. 10(b) is given by,

$$\log Ix = -8.34 + 1.50 \log A \; . \tag{4}$$

Interestingly, the X-ray peak flux is linearly related to the volume of the active region, because volume $\sim \mathrm{A}^{3/2}$. On the other hand, the CME speed (V km s^{-1}) and A in Fig. 10(c) are related by,

$$\log V = 2.54 + 0.22 \log A \; . \tag{5}$$

If the SEPs are accelerated by the CME-driven shock, the SEP intensity need not have a specific relationship with the active region area. Even though the CME is rooted in the active region, the three-dimensional shock front ahead of the CME, when it is within a few solar radii from the Sun, is much larger than the active region area. The SEPs are released from the shock front surrounding the moving volume of the CME. This might explain why there is no relationship between the SEP intensity and active region area. On the other hand, the flare is confined to the arcade of loops in the active region and filled with hot plasma emitting soft X-rays. The flaring loops are generally confined to the active region, so one can understand the good correlation between flare size and active region area. In other words, the flare energy and the SEPs

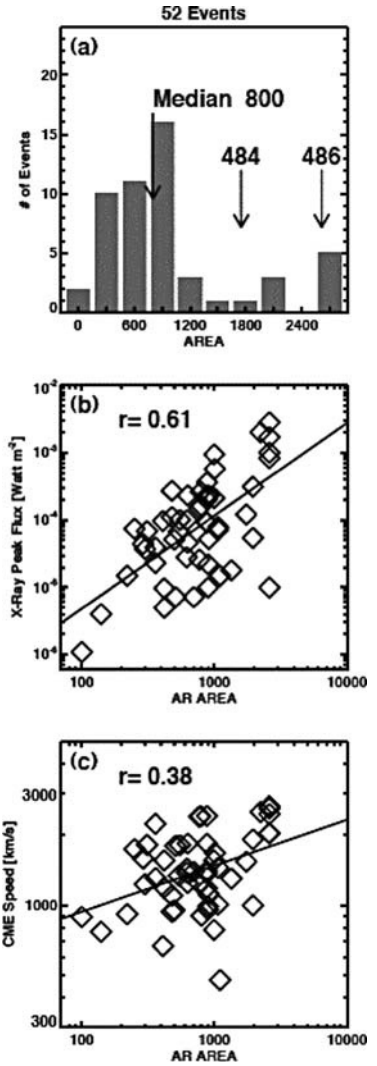

Fig. 10. (**a**) Distribution of active region areas associated with the LSEP events from 1996–2003. (**b**) scatter plot between X-ray flare size (measured as the peak intensity in the 1–8 Å GOES X-ray channel) and AR area. (**c**) scatter plot between CME speed and AR area. The corresponding correlation coefficients and regression lines are shown in (**b**) and (**c**). The two largest active regions 486 and 484 that produced some of the most intense events of cycle 23 are indicated in (**a**)

are released at two different spatial locations, on either side of the moving CME plasma. Yet, the three physical entities (CME, flare loops, and SEPs) seem to be related in a complex way. This result may also be relevant to the previous result that the intensity of energetic (108 keV) electrons are well

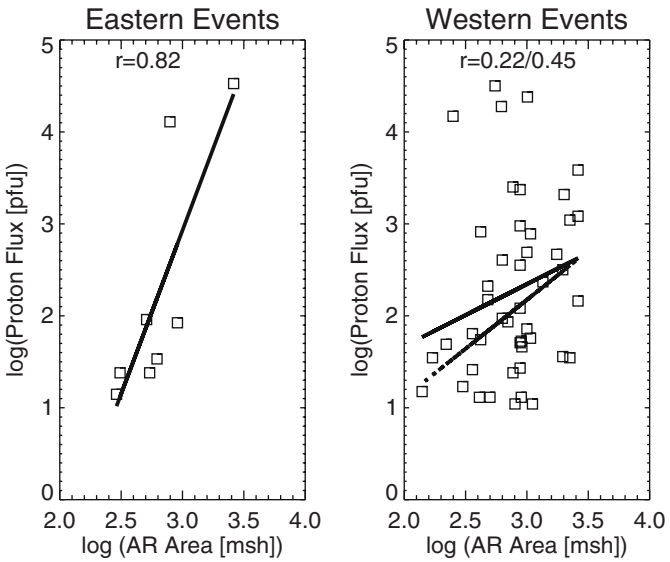

Fig. 11. Correlation between active region area (in millionths of solar hemisphere – msh) and the proton intensity (pfu) in logarithmic units. **Left**: Eastern events (8), **Right**: western events (46). The corresponding regression lines are also shown. For the western events, the lower straight line was obtained when the four outliers of very high intensity are excluded ($r = 0.45$)

correlated with flare size [10]. If these electrons propagating away from the sun are accelerated by the same process as that of the precipitating electrons, one might expect a good correlation with the flare size.

Figure 11 shows a scatter plot between the SEP intensity and active region area. The two quantities are only weakly correlated (correlation coefficient $r = 0.31$ for all the events), as was shown in [24]. When the events were separated into eastern and western events based on their source longitude, the correlation coefficient remained small ($r = 0.20$) for western events, while it became higher ($r = 0.82$) for the eastern events. However, the sample of eastern events is too small. If we exclude the four high-intensity western events, the correlation coefficient improved to $r = 0.45$. Thus there is an overall correlation between the SEP intensity and AR area, but weak.

8 Discussion and Conclusions

The possible non-existence of CMEless type II bursts and the association of progressively more energetic CMEs with metric, DH and full-range type II bursts suggests the importance of CMEs for the type II phenomena, and by extension, for the SEP events. There are several related issues that need to be addressed in the framework of CME-driven shocks.

For example, a significant fraction of fast and wide CMEs are not associated with any type II radio bursts above the detection threshold of radio instruments [15]. These radio-quiet CMEs pose a significant challenge to the CME-driven shock hypothesis. Furthermore, a large number of metric type II bursts and DH type II bursts are associated with slow CMEs (speeds < 400 km s^{-1}). This apparent paradox originates from the definition of fast and slow CMEs. Traditionally, CMEs faster than $\sim$400–500 km s^{-1} were thought to be fast because they are super-Alfvenic according to the canonical value of coronal Alfven speed used in the literature (see e.g., [26, 29]). This value may be generally true for regions above the source surface, but it may not be so in the coronal region where metric type II bursts originate. A careful look at the variation of density and magnetic field variation in the inner corona reveals that the Alfven speed could be as low as 200 km s^{-1} near the base of the quiet corona [39] with a peak of several hundred km s^{-1} around 3 $R_{\odot}$. This fact has been taken to suggest that flare blast waves should have speeds exceeding the Alfven speed peak to become interplanetary shocks [45]. Type II bursts mostly originate from the active region corona, so the Alfven speed profile must be modified by introducing the magnetic field of active regions [14]. The modified profile is similar to the quiet-sun profile except for the rapid increase towards the coronal base to a few thousand km s^{-1} at the core of the active region [14, 46]. Interestingly, CMEs start from rest at very small coronal heights before attaining significant speed. This combination of circumstances might explain the relatively low starting frequency of type II bursts because it is difficult to shock the core of the active region corona. Thus a 300 km s^{-1} CME could be a fast CME while a 1000 km s^{-1} CME could be a slow one depending on the value of the ambient Alfven speed. If this result is combined with the requirement that a CME needs to be present for a type II burst production, one can explain the type II phenomenon solely in terms of CME-driven shocks (see also [8, 25]). Such a conclusion would also be consistent with the idea that SEPs are due to CME-driven shocks. The close association between CMEs and type II bursts suggests that the associated flares need to be eruptive, i.e., they are associated with mass motion. This means the non-eruptive flares, which constitute the majority, are not associated with type II bursts.

While there is universal agreement that CME-driven shocks are responsible for the type II bursts in the interplanetary medium (varieties 2-6 in 2), there is no such agreement on those (variety 1 in 2) confined to the metric domain (see, e.g., [37]). It is often argued that the presence of a CME during a metric type II does not imply a physical relationship between the two phenomena (see, e.g., [62] and references therein). While this might become clear when CME observations extend to lower heights such as by the coronagraphs on board STEREO mission to be flown soon, the fact remains that even X-class flares do not produce type II bursts if they are non-eruptive (i.e., if they lack CMEs). As far as SEPs are concerned, purely metric type II bursts are unimportant.

The Alfven speed profile also provides a natural explanation for the CME interaction phenomenon in terms of a temporary change in the Alfven speed due to the presence of preceding CMEs. The density enhancement in the ambient medium caused by the preceding CMEs can temporarily reduce the Alfven speed, so that the shock entering such a CME will attain a higher Mach number and hence accelerate more particles. More electrons would imply higher intensity radio emission, as has been observed in the case of colliding CMEs. A generalized version of such CME interaction is the propagation of a CME-driven shock through a series of preceding CMEs of various sizes and amplitudes, i.e., enhanced turbulence. The opposite end of the density effect is to have a depletion in the ambient medium, which would result in weakening of the shock and consequently less number of particles would be accelerated. This would mean a weaker radio emission and less number of SEPs. Eruption near a coronal hole presents such a situation, because the flank of the shock nearer to the coronal hole is likely to be weaker than the opposite flank. The effect of the turbulence can also lead to severe distortion of the shock front causing corrugation as occasionally observed [1, 38]. Such an inhomogeneity in shock strength was also visualized early on and referred to as 'Swiss Cheese effect' [5].

One other consequence of the preceding CMEs is that they can accelerate particles to low levels, which may serve as seed particles for the follower shock. Most of the large SEP events are also accompanied by flares, which also accelerate particles. Flare-related impulsive events are of short duration, small in size, but more frequent. The CME-related gradual events are less frequent, but last longer and have much higher intensity. Although there are separate investigations of SEP seed particles [31] and flare seed particles [47] there is no systematic investigation to assess the relative importance of these two populations as seed particles. However, one can speculate that the SEP seed particles may contribute to the intensity of the resulting SEP event, while flare particles may alter the composition of the accelerated particle population.

Acknowledgments

I thank S. Yashiro and E. Aguilar-Roriguez for help with some figures. This material is based upon work supported by the National Aeronautics and Space Administration under the Living with a Star (LWS) and Supporting Research and Technology (SR&T) programs.

References

1. S. D. Bale, M. J. Reiner, J.-L. Bougeret et al.: Geophys. Res. Lett. **26**, 1573 (1999) 141, 158
2. J.-L. Bougeret, M. L. Kaiser, P. Kellogg et al.: Space Sci. Rev. **71**, 231 (1995) 142
3. J.-L. Bougeret, P. Zarka, C. Caroubalos et al.: Geophys. Res. Lett. **25**, 2513 (1998) 140

4. H. V. Cane and R.G. Stone: Astrophys. J. **282**, 339 (1984) 143, 146
5. J. K. Chao: In *Solar Wind Three*, ed by C. T. Russell (Univ. California Los Angeles, 1974), pp. 169–174 158
6. E. W. Cliver, D. F. Webb, R. A. Howard: Solar Phys. **187**, 89 (1999) 145
7. E. W. Cliver, S. W. Kahler, D. V. Reames: Astrophys. J. **605**, 902 (2004a) 146
8. E. W. Cliver, N. Nitta, B. J. Thompson, J. Zhang: Solar Phys. **225**, 105 (2004b) 157
9. I. J. D. Craig, Y. E. Litvinenko: Astrophys. J. **570**, 387 (2002) 140
10. N. Gopalswamy: Planetary and Space Sci. **52**, 1399 (2004a) 143, 145, 146, 156
11. N. Gopalswamy: A Global Picture of CMEs in the Inner Heliosphere, In: *The Sun and the Heliosphere as an Integrated System*, ed by G. Poletto and S. Suess (Kluwer, Berlin Heidelberg New York 2004b), pp. 201–252 143
12. N. Gopalswamy: Interplanetary Radiobursts. In *Solar and Space Weather Radiophysics*, ed by D. Gary and C. Keller (Kluwer, Berlin Heidelberg New York 2004c), pp. 305–333
13. N. Gopalswamy, M. L. Kaiser, R. P. Lepping, et al.: J. Geophys. Res. **103**, 307 (1998) 143
14. N. Gopalswamy, A. Lara, M. L. Kaiser, J.-L. Bougeret: J. Geophys. Res. **106**, 25261 (2001a) 143, 146, 157
15. N. Gopalswamy, S. Yashiro, M. L. Kaiser et al.: J. Geophys. Res. **106**, 29219 (2001b) 143, 157
16. N. Gopalswamy, S. Yashiro, M. L. Kaiser, et al.: Astrophys. J. Lett. **548**, L91 (2001c) 148
17. N. Gopalswamy, S. Yashiro, M. L. Kaiser et al.: Geophys. Res. Lett. **29**, 106 (2002a)
18. N. Gopalswamy, S. Yashiro, G. Michalek et al.: Astrophys. J. **572**, L103 (2002b) 148, 152
19. N. Gopalswamy: Geophys. Res. Lett. **30**, SEP1-1 (2003) 146
20. N. Gopalswamy, S. Yashiro, A. Lara et al.: Geophys. Res. Lett. **30**, SEP 3–1 (2003a) 147, 149, 152, 153
21. N. Gopalswamy, S. Yashiro, M. L. Kaiser, R. A. Howard: Adv. Space Res. **32 (12)**, 2613 (2003b) 140, 149
22. N. Gopalswamy, S. Nunes, S. Yashiro, R. A. Howard: Adv. Space Res. **34 (2)**, 391 (2004a)
23. N. Gopalswamy, S. Yashiro, S. Krucker et al.: J. Geophys. Res. **109**, A12105 (2004b) 147, 152
24. N. Gopalswamy, S. Yashiro, S. Krucker, R. A. Howard: CME Interaction and the Intensity of Solar Energetic Particle Events. In: *Coronal and Stellar Mass ejections, IAU Symposium No. 226*, ed by K. Dere, J. Wang and Y. Yan, pp. 367–373 (2005a) 147, 154, 156
25. N. Gopalswamy, E. Aguilar-Rodriguez, S. Yashiro et al.: J. Geophys. Res. **110**, A12, A12S07 (2005b)
26. J. T. Gosling, E. Hildner, R. M. MacQueen, et al.: Solar Phys. **48**, 389 (1976) 146, 157
27. D. Haggerty, E. Roelof: Astrophys. J. **579**, 841 (2002) 157
28. S. Hoang, J.-L. Steinberg, G. Epstein, et al.: J. Geophys. Res. **85**, 3419 (1980) 140
29. A. J. Hundhausen: J. Geophys. Res. **98**, 13177 (1993) 141
30. S. W. Kahler: Astrophys. J. **261**, 710 (1982) 157
31. S. W. Kahler: J. Geophys. Res. **106**, 20947 (2001) 146
32. S. W. Kahler, E. Hildner, M. A. I. van Hollebeke: Solar Phys. **57**, 429 (1978) 147, 153, 154,

33. S. W. Kahler, N. R. Sheeley, Jr., R. A. Howard, et al.: Solar Phys. **93**, 133 (1984) 146
34. S. W. Kahler, N. R. Sheeley, Jr., R. A. Howard, et al.: J. Geophys. Res. **89**, 9683 (1984) 145
35. M.-B. Kallenrode: J. Phys. G: Nucl. Part. Phys. **29**, 965 (2003) 147
36. K.-L. Klein, G. Trottet, H. Aurass, A. Magun, Y. Michou: Adv. Space Res. **17 (4–5)**, 247 (1996) 140
37. K.-L. Klein, J. I. Khan, N. Vilmer et al.: Astron. Astrophys. **346**, L53 (1999) 139
38. S. A. Knock, I. H. Cairns, P. A. Robinson, Z. Kuncic: J. Geophys. Res. **108 (A3)**, SSH6-1 (2003) 157
39. M. Krogulec, Z. E. Musielak, S. T. Suess, S. F. Nerney, R. L. Moore: J. Geophys. Res. **99**, 23489 (1994) 141, 158
40. A. Lara, N. Gopalswamy, S. Nunes, G. Muñoz, S. Yashiro: Geophys. Res. Lett. **30**, 8016 (2003) 157
41. R. P. Lin: Solar Flare Particles, in: *From the Sun: Auroras Magnetic Storms, Solar Flares, Cosmic Rays*, ed by S. T. Suess and B. T. Tsurutani, (American Geophysical Union, Washington, DC. 1998), pp. 91–102 142
42. R. P. Lin, S. Krucker, G. J. Hurford et al.: Astrophys. J. Lett. **595**, L69 (2003) 139
43. J. L. Lovell, M. L. Duldig, J. E. Humble: J. Geophys. Res. **103**, 23733 (1998) 150
44. H. H. Malitson, J. Fainberg, R. G. Stone: Astrophys. Lett. **14**, 111 (1973) 139
45. G. Mann, A. Klassen, C. Estel, B. J. Thompson: In: *Proc. of 8th SOHO Workshop*, ed by J.-C. Vial and B. Kaldeich-Schürmann. (ESA, 1999), p. 477 141
46. G. Mann, A. Klassen, H. Aurass, H.-T. Classen: Astron. Astrophys. **400**, 329 (2003) 157
47. G. M. Mason, J. E. Mazur, J. R. Dwyer: Astrophys. J. **525**, L123 (1999) 157
48. G. J. Nelson, D. B. Melrose: Type II bursts. In: *Solar Radiophysics*, ed by D. J. McLean and N.R. Labrum, (Cambridge University Press, Cambridge 1985), pp. 333–359 158
49. G. Newkirk: Astrophys. J. **133**, 983 (1961) 141
50. R. Payne-Scott, D. E. Yabsley, J. G. Bolton: Nature **160**, 256 (1947) 141
51. U. R. Rao, K. McCracken, R. P. Bukata: J. Geophys. Res. **72**, 4325 (1967) 141
52. D. V. Reames: Space Sci. Rev. **90**, 413 (1999) 141
53. D. V. Reames:Astrophys. J. **571**, L63 (2002) 140, 147
54. M. J. Reiner, M. Karlicky, K. Jiricka et al.: Astrophys. J. **530**, 1049 (2000) 140
55. N. R. Sheeley, Jr., R. A. Howard, D. J. Michels et al.: Astrophys. J. **279**, 839 (1984) 140
56. G. M. Simnett, E. C. Roelof, D. K. Haggerty: Astrophys. J. **579**, 854 (2002) 145
57. E. J. Smith, R. G. Marsden, A. Balogh et al.: Science **302**, 1165 (2003) 140
58. R. T. Stewart, R. A. Howard, F. Hansen et al.: Solar Phys. **36**, 219 (1974) 141, 142
59. Z. Svestka, L. Fritzova-Svestkova: Solar Phys. **36**, 219 (1974) 145
60. J. Torsti, L. Kocharov, J. Laivola: Astrophys. J. **573**, L59 (2002) 146
61. B. Vrsnak, V. Ruzdjak, P. Zlobec, H. Aurass: Solar Phys. **158**, 331 (1995) 140
62. B. Vrsnak, A. Warmuth, M. Temmer et al.: Astron. Astrophys. **448**, 739 (2006) 141
63. J. P. Wild, L. L. McCready: Austral. J. Sci. Res. **A3**, 387 (1950) 157
64. R. Woo, J. W. Armstrong: Nature **292**, 608 (1981) 141